Lipidomic Profiling Reveals Shared and Distinct Pathological Signatures in Sporadic Parkinson's Disease and GBA Mutation Carriers: Implications for Disease Mechanisms

Sonia Sanz Muñoz[1#], Frederik Ravnkilde Marlet[1#], Mesut Bilgin[2], Jesper E Dreier[1], Erwan Bezard[3], Benjamin Dehay[3], Zane Jaunmuktane[4,5], Kenji Maeda[6], Céline Galvagnion[1*]

[1] Department of Drug Design and Pharmacology, Faculty of Health and Medical Sciences, University of Copenhagen, 2100, Copenhagen, Denmark

[2] Lipidomics Core Facility, Danish Cancer Institute, Copenhagen, Denmark

[3] Univ. Bordeaux, CNRS, IMN, UMR 5293, F-33000 Bordeaux, France

[4] Division of Neuropathology, National Hospital for Neurology and Neurosurgery, University College London Hospitals NHS Foundation Trust, London, UK

[5] Queen Square Brain Bank for Neurological Disorders and Department of Clinical and Movement Neurosciences and Queen Square Brain Bank for Neurological Disorders, UCL, Queen Square Institute of Neurology, London, UK

[6] Cell Death and Metabolism group, Center for Autophagy, Recycling and Disease, Danish Cancer Institute, Copenhagen, Denmark

# SSM and FRM contributed equally

* Email to: celine.galvagnion@sund.ku.dk

Abstract

Parkinson's Disease (PD) is a neurodegenerative disorder characterised by the deposition of protein inclusions, called Lewy Bodies (LBs), in neurons. LBs are heterogeneous structures whose main constituent is the protein alpha-synuclein (αS) and that are also composed of lipid molecules. Disruptions in the levels of specific lipids, including sphingolipids, fatty acids, and cholesterol, have been associated with PD, suggesting a role of lipids in the emergence and spreading of αS and PD pathology. Using a combination of shotgun lipidomics and biochemical analyses of PD amygdala homogenates, we have shown that long sporadic disease duration and *GBA* risk mutation are associated with a decrease in the protein and activity levels of glucocerebrosidase (GCase) activity and in cardiolipin levels and an increase in those of pathological αS, cholesterol, diacylglycerides, sphingolipids and specific glycerophospholipids (GPL). Long sporadic PD and GBA risk mutations also led to a shift from long unsaturated to short saturated GPL and from short to long sphingomyelin and ceramide. Moreover, the levels of lipid classes and species affected by long sPD and *GBA* risk mutations were found to correlate negatively with GCase activity and positively with pathological αS levels. We found that *GBA* mutation with mild phenotype affects lipid levels in the same direction as *GBA* risk mutation and long sPD but to a lesser extent and that *GBA* mutation carriers with severe phenotype led to changes in the opposite direction for the same lipids. Finally, the lipid analyses of LB- and small aggregates enriched fractions show that long sPD and *GBA* risk mutations led to the same changes in the levels and species distribution of GPL and SL than in homogenates but to a lesser extent. Together, these results suggest the need for patient stratification in clinical trials of therapeutic interventions in PD-GBA and that successful therapeutics against PD-GBA should be considered for sporadic PD.

Introduction

Parkinson's disease (PD) is a neurodegenerative disorder characterized by the loss of dopaminergic neurons and the deposition of protein-lipid co-assemblies called Lewy bodies (LBs)[1,2]. These LBs are composed of protein and lipid molecules including organelles and their main constituent is alpha-synuclein (αS)[2,3]. αS is a small (14.5 kDa) intrinsically disordered protein proposed to play a role in synaptic plasticity via binding to synaptic vesicles[4–7]. αS-membrane binding is associated with the folding of the protein into an alpha-helix, and several studies have shown that this protein-membrane interaction is crucial for the proposed biological function of αS, but also for modulating the formation by the protein of toxic amyloid fibrils[6–13]. Indeed, αS can bind membranes of different lipid compositions but only co-assemble into mixed lipid-protein amyloid fibrils with a specific set of lipids, including negatively charged phospholipids and gangliosides, at high protein-to-lipid ratios[9,13–16].

Disruptions in the levels of specific lipids have been observed in association with both the sporadic and familial forms of PD[17,18]. Mutations in the *GBA* gene that encodes the lysosomal glycoprotein glucocerebrosidase (GCase) are the most important genetic risk factor for PD[19–21]. *GBA* mutations can be classified as severe, mild, or at risk depending on the associated severity of the phenotype [22–25] and were found to lead to a decrease in GCase activity in patient-derived samples, including post-mortem brain samples (i.e. cerebellum, putamen, amygdala, substantia nigra (SN) and cingulate gyrus)[18], cerebrospinal fluid (CSF)[26], fibroblasts[27–31] and induced pluripotent stem cell-derived neurons[26,31–36]. A decrease in GCase activity due to *GBA* mutations or small molecule inhibitor treatments (e.g. conduritol-β-epoxide) were reported to be associated with increased levels of total and pathological αS and / or GCase lipid substrates, glucosylceramide (GlcCer) and glucosylsphingosine (GlcSph), in cellular and animal models of PD and in patient-derived samples[18].

GCase activity has been found to decrease in association with aging in healthy and PD brains and with PD carriers and non-carriers of *GBA* mutation, i.e. PD-GBA and sPD cases, respectively[18]. The magnitude of this decrease and that of the associated increase in the lipids and total/pathological αS were reported to vary from one brain area to another and from one cohort to another[18]. GCase activity decreased with aging in healthy SN and putamen and in PD SN[37,38], and such a decrease in GCase activity was associated with increased levels of pathological αS and GlcCer only in PD SN[38]. Studies comparing GCase activity in sPD and healthy controls gave conflicting results where GCase activity was reported to be either significantly decreased or unchanged in the cerebellum, cingulate cortex,

putamen and SN but to be systematically unaffected in frontal and occipital cortices[18,39]. Such a decrease in GCase activity was not consistently associated with increased GCase lipid substrates, GlcCer and GlcSph[18]. An increase in gangliosides and other sphingolipids in some brain areas has been reported to a variable extent among different cohorts. No changes in GlcCer or GlcSph were reported in the cerebellum and putamen[40] and temporal cortex of patients with sPD or PD-GBA[41]. In contrast, increased levels of GlcCer were reported with age in PD SN[38].

In this study, we investigated the correlations between the levels of GCase protein and activity, pathological αS, and lipids in amygdala homogenates of PD patients with different disease duration and PD patients carrier of different types of *GBA* mutations (severe, mild and risk) using a combination of biochemical and lipidomic analyses. We found that the levels of GCase protein/activity and cardiolipin were decreased whereas those of total and pathological αS, free cholesterol (Chol), diacylglycerides (DAG), sphingolipids (SL) and specific glycerophospholipids (GPL), were increased in sPD cases with disease duration > 30 y, "long sPD" cases, compared to sPD cases with disease duration < 30y. Furthermore, our shot-gun lipidomic analyses show that long sPD disrupts the species distribution of GPL and SL and led to shift towards shorter and more saturated GPL and towards longer and more unsaturated sphingomyelin and ceramide. Moreover, we discovered that *GBA* mutations affect the levels GCase activity/protein, total and pathological αS and lipids to different extents. *GBA* risk mutations led to the same changes in the levels and species distribution of the same lipids as those observed for long sPD. *GBA* mutations with mild phenotype led to similar lipid changes as those observed for *GBA* risk and long sPD, but to a lesser extent. However, *GBA* mutation with severe phenotype affected less lipids and led to changes in their levels and species distribution in the opposite direction to that observed for *GBA* mild and risk mutations and long sPD. Finally, the biochemical and lipidomic analyses of fractions enriched in LBs or small aggregates (SA) show that the levels of GCase activity/protein as well as those of pathological αS did not differ among the different groups studied (i.e. sPD with different disease durations and the three PD-GBA groups) and that long sPD and *GBA* risk mutations mainly affected the levels and species distribution of SL in the same directions as those observed for the corresponding PD amygdala homogenates.

Results

Long sPD is associated with (i) a decrease in GCase activity, (ii) a decrease in GCase protein levels, and (iii) an increase in pathological αS in PD amygdala homogenates

To investigate the effect of disease duration on the lipidome of amygdala and its composing LBs and SAs, we examined 4 groups of sPD patients with different disease duration: < 10 years (y) (n = 4), 10 – 20 y (n = 6), 21 – 30 y (n = 5) and > 30 y (n = 5). These patients did not differ significantly in their age at death but in their age of onset (Table 1). Furthermore, we selected the amygdala because of its high αS pathology burden in the majority of PD case, contributing to PD non-motor symptoms [42–44]. We found that GCase activity decreased significantly with disease duration not in a linear but rather a stepwise manner (**Fig. 1a**) and was ca. 50% lower in amygdala homogenates of sPD cases with disease duration longer than 30 y (long sPD, $sPD_{>30y}$) compared to cases with disease duration less than 30 y ($sPD_{<30y}$) (**Fig. 1a,b**). GCase protein levels followed the same trend among the four disease duration groups (**Fig. 1c** and **Fig. S1**). They were also decreased by ca. 50% in long sPD compared to $sPD_{<30y}$ amygdala homogenates (**Fig. 1d**). We did not observe significant changes in GCase activity and protein levels between males and females among the sPD cases (**Fig. S2**). The observed decrease in both GCase activity and protein levels were associated with increased levels of pathological αS (**Fig. 1e,f**). Our western blot analyses show the presence of monomeric αS on the membrane stained with Syn1 antibody (total αS) and a multitude of species with molecular weight (MW) above 14 kDa on the membrane stained with phosphorylated Ser 129 antibody (pSer-αS) (**Fig. 1e,f and Fig. S1**). We chose to express pathological αS using the following ratios: (i) the level of total phosphorylated αS on Ser-129 (pSer-αS) (all bands; **Fig. S1**) relative to that of total αS (all bands; **Fig. S1**) and (ii) the levels of High MW (HMW) pSer-αS (bands with MW > 14 kDa; **Fig. S1**) relative to the monomeric pSer-αS (bands at 14 kDa, gels; **Fig. S1**) referred to as pSer-αS (i) and HMW pSer-αS (ii), respectively, in the rest of the manuscript. The levels of pSer-αS and HMW pSer-αS were significantly higher in long sPD compared to $sPD_{<30y}$ cases (**Fig. 1e,f**). Moreover, pSer-αS but not HMW pSer-αS correlate negatively with GCase activity levels (**Fig. 1g**), and none of them correlate with the levels of GCase protein (**Fig. 1h**).

Long sPD is associated with (i) an increase in total lipid level and in those of sphingolipids, DAG, cholesterol, and specific glycerophospholipids and (ii) a change in their chain properties in PD amygdala homogenates

In light of these results, we investigated the effect of a decrease in GCase activity and protein levels associated with long sPD on the lipidome of PD amygdala homogenates using mass-spectrometry-based shotgun lipidomics. 306 lipid species were detected, and an average of 25,857 (± 10,128) pmol per 25 µg protein was present in the homogenates. Homogenates were composed of the 55% sterols

(inc. 55% Chol + 0.1% cholesteryl ester (CE)), 38% GPL, whose main classes were phosphatidylcholine (PC) (20%), ether phosphatidylethanolamine (PE O-) (7.7%), PE (3.7%), phosphatidylserine (PS) (2.1%), lyso-PE (1.1%) and phosphatidylinositol (PI) (1.0%), 6.9% SL (inc. sphingomyelin (SM) (4.4%), Hexosylceramide (HexCer) (1.4%), ceramide (Cer), (0.5%), sulfatides (SHexCer) (0.3%) and diHexCer (0.3%)) and 0.2% DAG (**Fig. 1i,j**).

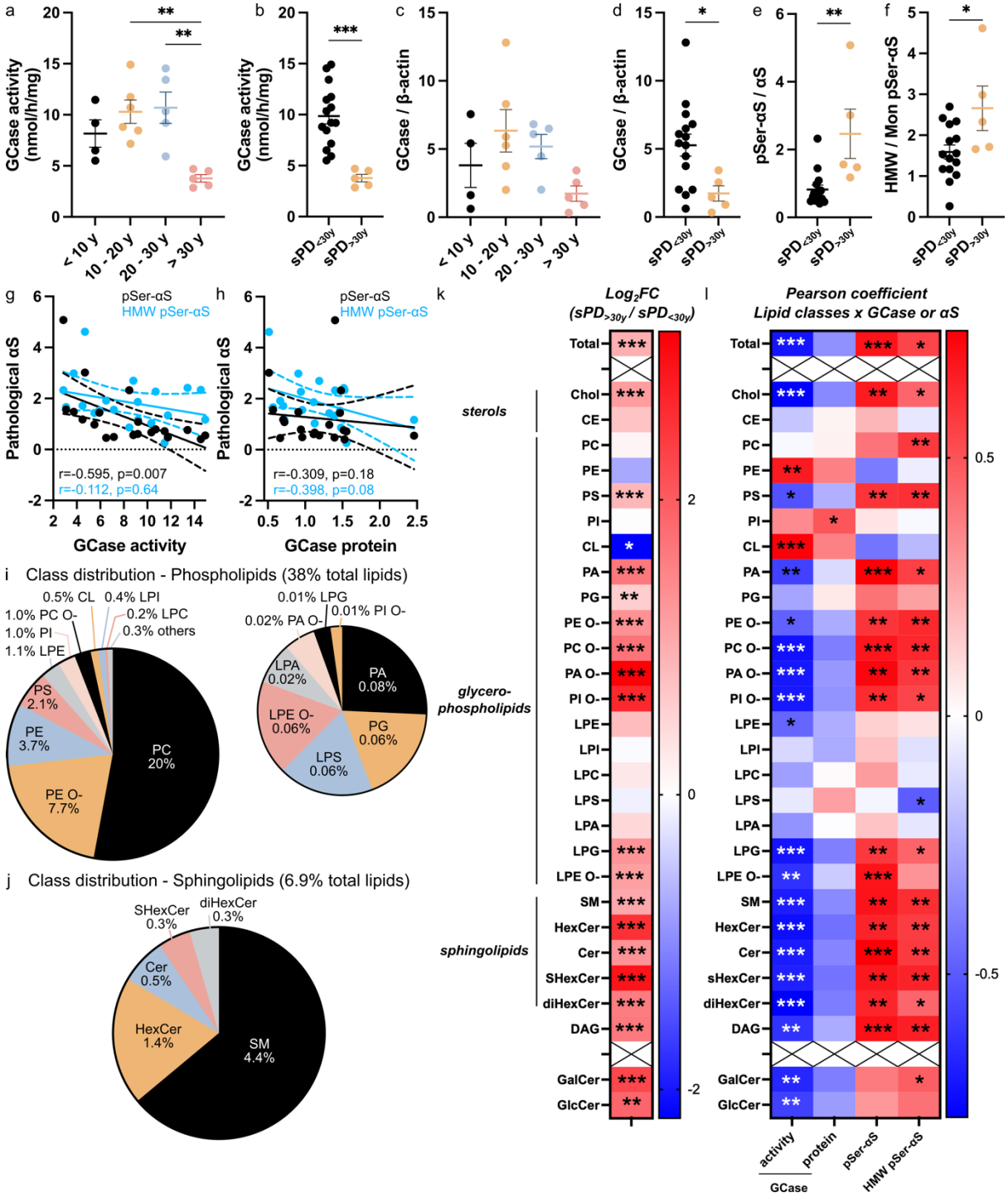

Figure 1: The levels of GCase activity and protein, pathological αS and lipid classes are affected by sPD duration and correlate between each other in PD amygdala homogenates. a,c. Levels of GCase activity (a) and GCase protein (c) measured in amygdala homogenates from patients with disease duration ranging from < 10 y (n = 4), 10 – 20 y (n= 6), 21

– 30 y (n = 5) and > 30 y (n = 5). One-way ANOVA with Šidák, multiple comparisons of each mean with the mean of every other group. b,d. Levels of GCase activity (b) and GCase protein (d) measured in amygdala homogenates from $sPD_{<30y}$ (n = 15) and $sPD_{>30y}$ (n= 5) sPD cases. t-test comparison. e,f. Levels of pSer-αS / αS (e) and of HMW / Monomer (pSer-αS) (f) measured in amygdala homogenates from $sPD_{<30y}$ (n = 15) and $sPD_{>30y}$ (n= 5) sPD cases. t-test comparison between the mean of $sPD_{<30y}$ vs that of $sPD_{>30y}$. g,h. Variation in the levels of pSer-αS / total αS (black) and of HMW / Monomer pSer-αS (blue) with those of GCase activity (g) and protein (h). The solid line shows simple linear regression to test the association between the levels of pSer-αS / αS (black) or HMW / Monomer pSer-αS (blue) with those of GCase activity (g) or GCase protein (h). i,j. Distribution of glycerophospholipids (i) and sphingolipids (j) in amygdala homogenates from sPD cases. k. Heat maps showing log_2FC in the levels of lipid classes associated with long sPD. The asterisks indicate the p-value for the t-test comparison $sPD_{<30y}$ (n = 15) vs $sPD_{>30y}$ (n = 5) cases. *p<0.033, **p<0.002, ***p<0.001. l. Heat map showing the Pearson r coefficient for the correlation between the levels of each lipid class and GCase activity or protein or total or HMW pSer-αS in PD amygdala homogenates. *p<0.033, **p<0.002, ***p<0.001.

Lipid levels were normalized to the protein content of the samples and expressed as pmol per µg of protein for direct comparison. Figure 1k shows the log_2 fold change (log_2FC) in the level of each lipid class (e.g. PC, PE, HexCer…) associated with long sPD, with $log_2FC = log_2\left(\frac{pmol\ of\ a\ given\ lipid\ class\ in\ sPD_{>30y}}{pmol\ of\ a\ given\ lipid\ class\ in\ short\ sPD_{<30y}}\right)$ (**Fig. 1k**). As expected for samples with decreased GCase activity levels, we observed increased levels of HexCer (composed of GlcCer, GCase lipid substrate, and GalCer) in $sPD_{>30y}$ cases relative to those in $sPD_{<30y}$ cases (**Fig. 1 k**). We performed LC-MS analyses of HexCer to purify and quantify GlcCer and GalCer and found that HexCer was composed of 90% GalCer and 10% GlcCer, in agreement with previously reported GlcCer/GalCer distribution of brain HexCer[45]. As observed for HexCer, the levels of both GlcCer and GalCer were increased in long sPD cases (**Fig. 1k**). The increase in lipid levels associated with long sPD was not limited to HexCer (GlcCer and GalCer) but extended to all other SL classes, i.e. SM, Cer, diHexCer and SHexCer. On the other hand, while cholesterol followed the same trend as that observed for SLs, GPL classes were either unchanged, increased or decreased, with the major GPL class PC being unchanged while PS and PEO- were increased and mitochondrial CL was decreased in long PD cases relative to those in $sPD_{<30y}$ cases. We note that mitochondrial PE showed a decreasing trend, although not significant. Finally, we found that the total lipid level also increased in long sPD cases (**Fig. 1k**).

Each lipid class is characterised by hydrocarbon chains that differ in the number of their carbons and double bonds (DB). We then investigated whether the observed changes in the levels of lipid classes due to long PD were accompanied by changes in the species distribution of these classes. Figure 2 and S3 show the species distribution of all SL and GPL for patients with disease duration below 30 y and above 30 y. For the SL, long PD mainly affected 36:1 and 42:2 species, whose levels were altered in opposite direction for HexCer/diHexCer, on one hand, and SM/Cer, on the other hand (**Fig 2a-f**). The largest changes were observed for SM and Cer for which 36:1 species were decreased and 42:2 species were increased in long PD cases relative to those in $sPD_{<30y}$ cases (**Fig. 2a-f**). For the GPL

species, we observed that long sPD led to a shift in their hydrocarbon chains towards more saturated and shorter ones mainly due to decreased levels of 40:6 species for PE, PS and PA and 40:7 species in PE O- and increased levels of 36:1, 36:2 and/or 36:3 species for PE O-, PE, PS, PA and PG (**Fig. 2g-k and S3**).

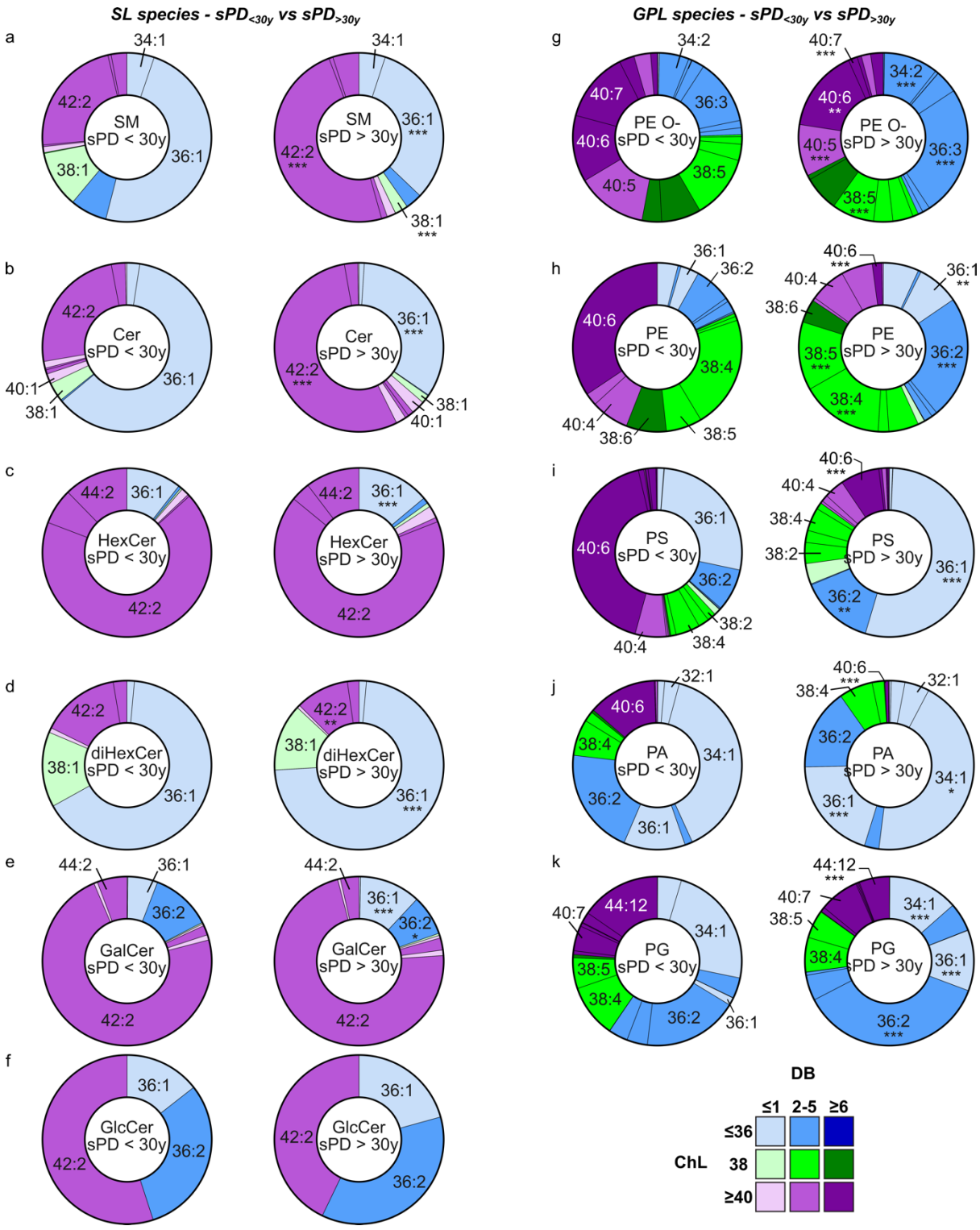

Figure 2: Long sPD leads to a shift from long to short GPL and from short to long SM and Cer. a-f. Pie charts showing the species distribution for SM (a), Cer (b) and HexCer (c), diHexCer (d), GalCer (e) and GlcCer (f) in sPD$_{<30y}$ (left) and

$sPD_{>30y}$ (right) cases. g-k. Pie charts showing the species distribution for PE O- (g), PE (h), PS (i), PA (j) and PG (k) in $sPD_{<30y}$ (left) and $sPD_{>30y}$ (right) cases. The asterisks indicate the p-value for two-way ANOVA with Šidák multiple comparison t-test between the mean of $sPD_{<30y}$ and that for $sPD_{>30y}$ for each lipid specie. *p<0.0332, **p<0.0021, ***p<0.0002.

Such changes in the distribution of species associated with long sPD translated into changes in the average chain length (ChL) and number of DB of the corresponding lipid class; we define hydrocarbon chain as the hydrocarbon chains of long-chain sphingoid bases and N-acyl group for SL and acyl and alkyl chains for GPL and ChL and DB as the total number of carbons and DB, respectively, in the hydrocarbon chain. Both the ChL and DB were systematically decreased for most GPL whereas they were found to be either increased for SM and Cer or decreased for HexCer and diHexCer in $sPD_{>30y}$ compared to their values in $sPD_{<30y}$ cases (**Fig. S4**).

Altogether, these results show that long sPD is associated with increased levels of specific GPL, all SL, DAG and Chol and decreased levels of CL in PD amygdala homogenates. Long sPD also affects the chain properties of these lipids and was found to lead to more SM and Cer, with longer chains, and to GPLs with shorter chains and reduced number of DB.

The levels of lipids affected by long sPD correlate with those of GCase activity and pathological αS in PD amygdala homogenates

In light of these results, we tested the correlation between the levels of lipid classes and those of GCase activity, GCase protein, and pathological αS measured in amygdala homogenates of sPD cases. The heat map in **Fig. 1l** shows the Pearson coefficient for these correlations, and the asterisks indicate the p-value and, thus, the significance of each correlation. We found that the total lipid levels, as well as those of the lipids that were increased due to long sPD (i.e., Chol, DAG, most phospholipids, and all SL), correlate both negatively with GCase activity and positively with pathological αS (**Fig. 1l**). On the contrary, the levels of lipids that were decreased due to long sPD (i.e. CL and PE) correlated positively with GCase activity and negatively with pathological αS (**Fig. 1l**). The same trend was observed with lipid species: the levels of lipid species that were significantly increased in association with long sPD (e.g., 36:1 species for PS, PA, HexCer, diHeCer and GalCer, 36:2 species for PE and PG, 36:3 species for PE O- and 42:2 species for Cer, and SM) all correlated both negatively with the levels of GCase activity and positively with the levels of pathological αS whereas the levels of lipid species that were significantly decreased in association with long sPD (e.g., 36:1 species for SM and Cer, 40:6 species for PE, PS and PA, 40:7 PE O-, 44:12 PG) all correlated both positively with those of GCase activity and negatively with those of pathological αS (**Fig. S5 and S6**). Finally, we found that ChL and DB that

were significantly decreased due to long sPD (i.e., most GPL, HexCer, diHexCer, and GalCer) all correlate both positively with GCase activity and negatively with pSer-αS whereas ChL and DB that were increased due to long sPD, i.e., SM, Cer, and DAG, all correlate negatively with GCase activity and positively with pSer-αS (**Fig. S4**).

Altogether, these results show that the levels of GCase activity and pathological αS correlate in opposite directions with the levels of lipid classes (all SL, Chol, DAG, and specific phospholipids) and lipid species affected by long sPD in PD amygdala homogenates.

GBA risk variant leads to the same changes in the levels of GCase activity and protein, αS, and lipids as those associated with long sPD

We then investigated the effect of *GBA* severe (p.L483P), mild (p.N409S) and risk (p.E365K, p.T408M) mutations on the levels of GCase activity/protein, pathological αS, and lipids in PD amygdala homogenates. *GBA* mutations led to a 50% decrease in the levels of GCase activity (significant for mild and risk *GBA*) compared to disease duration-matched sPD (sPD_{ddm}), a similar reduction to that associated with long sPD. Still, they did not alter significantly the levels of GCase protein (**Fig. 3a,b**). Such a decrease in GCase activity was associated with an increase in the levels of total pSer-αS only in *GBA* risk homogenates (**Fig. 3c,d**). Although the GCase activity/protein levels were similar for male and female sPD cases, we observed a significantly lower GCase protein value in male than in female PD-GBA cases (**Fig. S2**). The significantly lower value of GCase protein in male than in female cases was also observed when pooling all 35 PD cases (sPD + PD-GBA cases) (**Fig. S2**). We then investigated potential lipid changes associated with each of the three groups of *GBA* mutations by comparing the levels of lipid classes in amygdala homogenates from *GBA* mutation carriers to those of sPD_{ddm} cases (**Fig. 3e**). Even though the levels of GCase activity were decreased in amygdala homogenates for *GBA* mild, severe and risk carriers compared to sPD_{ddm} cases, only *GBA* risk mutation was associated with an increase in the total lipid levels, and the levels of Chol, DAG, the negatively charged GPL PS and PA, all ether-linked GPL and all SL when compared to the corresponding levels in sPD_{ddm} cases (**Fig. 3e**). Noteworthy, the lipid classes significantly affected by the *GBA* risk mutation, and the direction of the change were the same as those associated with long sPD (**Fig. 1g**). None of the lipid classes were affected by *GBA* severe and mild mutations (**Fig. 3e**). However, we observed the same trend in lipid changes for *GBA* mild as that described for *GBA* risk and an opposite trend in lipid

changes for *GBA* severe (**Fig. 3e**). The three types of *GBA* mutations also affected the species distribution of different lipid classes.

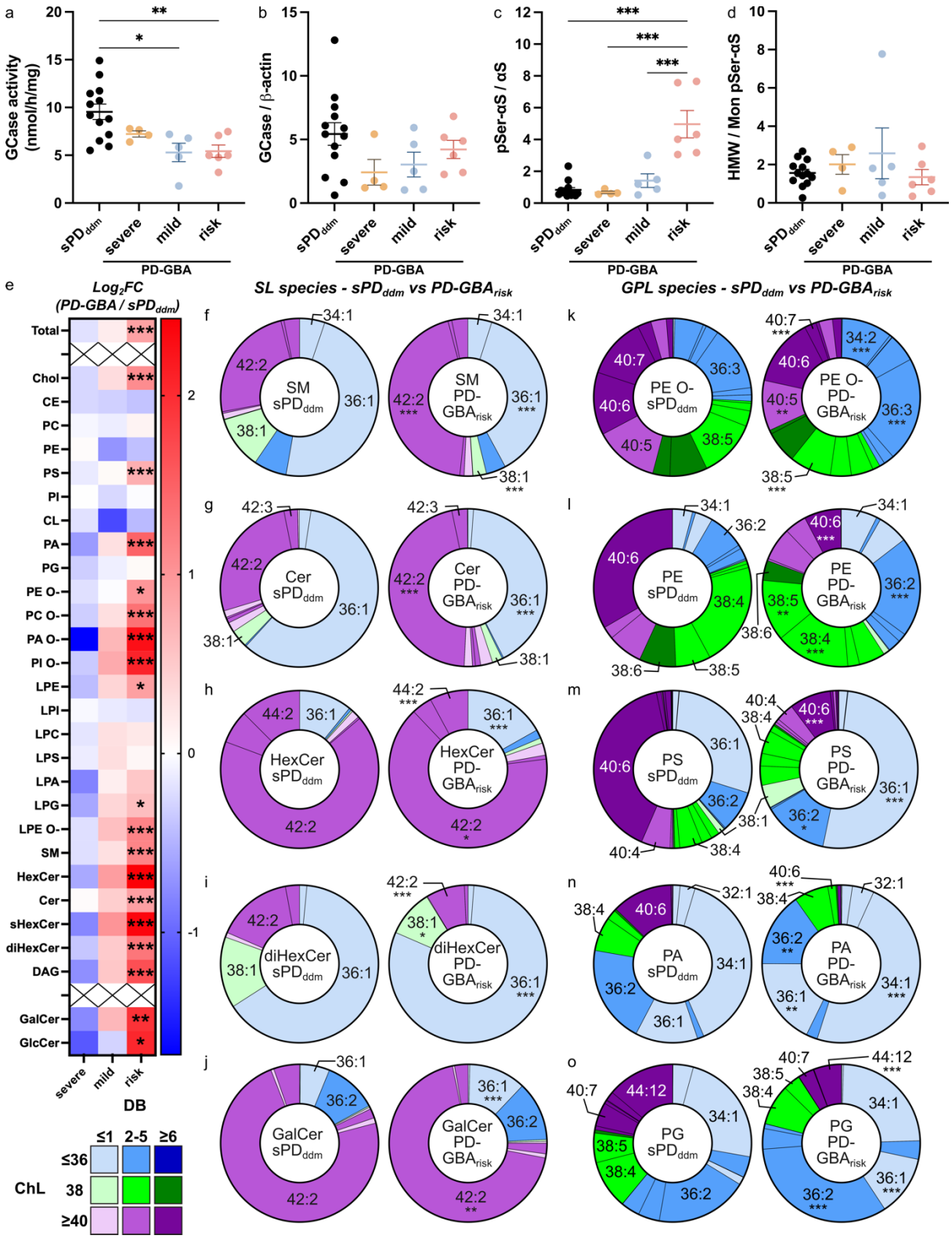

Figure 3: *GBA* risk mutations lead to a significant decrease in the levels of GCase activity/protein, an increase in pathological αS and to similar changes in the lipidome of PD amygdala to those observed in long sPD. a,d. Levels of GCase activity (a) and protein (c), total (c), and HMW (d) pSer-αS measured in amygdala homogenates from PD patients carrier of *GBA* severe (PD-GBA$_{severe}$, n = 4) or mild (PD-GBA$_{mild}$, n = 5) mutations or risk variants (PD-GBA$_{risk}$, n = 6) and disease duration-matched sPD (sPD$_{ddm}$) patients (n = 13). One-way ANOVA with Šidák multiple comparisons of each

mean with the mean of every other group. e. Heat maps showing log_2FC in the levels of lipid classes associated with *GBA* severe or mild mutations or *GBA* risk variant. The asterisks indicate the p-value for the t-test comparison *GBA* (severe (n = 4), or mild (n = 5) or risk (n = 6)) vs sPD_{ddm} (n = 13). f-j. Pie charts showing the species distribution for SM (f), Cer (g), HexCer (h), diHexCer (i), GalCer (j), PE O- (k), PE (l), PS (m), PA (n) and PG (o) in sPD_{ddm} (left) and PD-GBA_{risk} (right) cases. The asterisks indicate the p-value for two-way ANOVA with Šidák multiple comparison test between the mean of a specie level expressed in % of total class for PD-GBA_{risk} and that for sPD_{ddm} for each lipid specie. *p<0.0332, **p<0.0021, ***p<0.0002

GBA risk mutation led to the same changes in the species distribution of GPL and SL as those observed for long sPD, i.e. a decrease in 40:6 or 40:7 GPL species and an increase in 36:1, 36:2 or 36:3 GPL and a decrease in 36:1 SM/Cer and 42:2 HexCer/diHexCer and an increase in 36:1 HexCer and 42:2 SM/Cer (**Fig. 3 and S7**). As a result, *GBA* risk mutation led to the same changes in the average ChL and DB as those associated with long sPD (**Fig. S8**). *GBA* mild mutation was associated with the same changes in the levels of the same GPL and SL species, but to a lesser extent, as those reported for *GBA* risk mutation; mainly the levels of 40:6 or 40:7 GPL species were decreased and the levels of 42:2 SM/Cer were increased in PD-GBA mild cases relative to those in sPD_{ddm} cases (**Fig. S7**). Finally, we found that *GBA* severe mutation affected the same GPL and SL species, but to an even lesser extent, than those observed for *GBA* mild and risk but led to opposite changes in their levels (**Fig. S9**). For ex, we found that the levels of 36:1 SM/Cer and 40:6 PS were increased in PD-GBA_{severe} cases but decreased in PD-GBA_{mild} and PD-GBA_{risk} and the levels of PE O- 36:3 were decreased in PD-GBA_{severe} cases but increased in PD-GBA_{risk} and PD-GBA_{mild} (**Fig. S9**).

Altogether, these results show that, of the three different *GBA* mutation categories, only *GBA* risk variant is associated with a combined significant decrease in the levels of GCase activity, an increase in the levels of pathological αS and an increase in total lipid levels as well as those of Chol, DAG, some GPL, all ether-linked GPL, and all SL relative to those in sPD_{ddm} cases. Moreover, *GBA* risk mutations led to the same imbalance in the species distribution of these lipid classes as that observed for long sPD, i.e. a shift from long more unsaturated to short more saturated GPL and a shift from shorter to longer SM and Cer. The magnitude and direction of the changes in the levels of GCase activity, pathological αS, and lipids are the same for long sPD and *GBA* risk, suggesting that the lipid disruptions due to long sPD are likely to be the same as those associated with PD-GBA_{risk}. Finally, we found that the *GBA* mild mutation is associated with similar changes in the levels of GPL and SL species as for *GBA* risk, but the opposite is observed for *GBA* severe mutation. These results suggest that, even though GCase activity is decreased to a similar extent by the three types of *GBA* mutations, the different GBA mutations lead to different changes in the PD brain lipidome.

The lipid and αS composition of SAs and LBs is more homogenous among the different forms of Parkinson's Disease than that of homogenates

We then determined the lipid compositions and GCase and αS levels of amygdala homogenate fractions enriched in LBs or SAs from the sPD and PD-GBA cases. SAs and LBs were isolated using a sucrose gradient fractionation, as previously validated[46–49], with SA- and LB-containing fractions being recovered at the 1.2/1.4 M interface and 1.4/2.2 M interface, respectively (**Fig. S10a**). The fractions containing these insoluble αS protein aggregates/deposits were screened and identified by filter retardation assay (**Fig. S10b**). The LB-enriched fraction consisted of structures with a ca. 10 µm large diameter that are thioflavin S-positive (**Fig. S10c**). Both GCase and αS were further detected in LB- and SA-enriched fractions by immunodetection (**Fig. S11 and S12**). Two αS bands, one at ca. 45 kDa (50 kDa for pSer-129-αS and 45 kDa for αS) and one at 14.5 kDa, showed the highest intensities among the different bands detected for phosphorylated and non-phosphorylated αS, respectively, in both the LB- and SA-enriched fractions (**Fig. S11 and S12**, respectively). The pSer-αS and HMW pSer-αS levels were quantified using the same analysis as that described for the homogenates. In the LB-enriched fractions, the levels of GCase activity and protein were significantly decreased by half in long sPD cases compared to the value in $sPD_{<30y}$ cases (**Fig. S10d,f**) and were unaffected by *GBA* mutations (**Fig. S10e,g**). Among the LB-enriched fractions from the different groups (sPD and PD-GBA), the only significant changes in the levels of pathological αS were observed for the *GBA* risk group, where total pSer-αS levels were increased compared to sPD_{ddm} (**Fig. S10h-k**). For the SA-enriched fractions, the levels of GCase protein/activity as well as those of pathological αS were similar among the different groups (i.e. sPD and PD-GBA cases (**Fig. S10l-s**)).

We then determined the lipid composition of LB- and SA-enriched fractions and compared it to that of homogenates (**Fig. 4**). 181 and 257 lipid species were identified in LB- and SA-enriched fractions, respectively. An average of 4,704 +/- 1,525 pmol per 25 µg protein and 8,115 +/- 2,315 pmol per 20 µg protein were present in LB- and SA-enriched fractions, respectively. LB-enriched fractions were composed of 39% sterols (inc. 38% Chol and 1% CE), 55% GPL, whose main classes were PC (36%), PE (6.4%), PE O- (6.1%), PS (2.1%), lyso-PE (1.7%) and PI (1.7%), 4.9% SL (inc. SM (4.5%), HexCer (0.3%), Cer (0.5%), SHexCer (0.1%) and diHexCer (0.1%)) and 0.1% DAG (**Fig. 4a,b**); whereas SA-enriched fractions were composed of 31% sterols (inc. 30.9% Chol and 0.1% CE), 64% GPLs, whose main classes were PC (29%), PE O- (13%), PE (11%), PS (3.5%), and PI (3.2%), 4.8% SL (inc. SM

(3.8%), HexCer (0.2%), Cer (0.5%), SHexCer (0.1%) and diHexCer (0.1%)) and 0.1% (DAG) (**Fig. 4c,d**). We found that both LB- and SA-enriched fractions had higher percentages of PC and PE and lower percentages of Chol, diHexCer, HexCer and SHexCer compared to homogenates. SA-enriched fractions had specifically higher percentage of CE, PC, PE and PI (**Fig. 4e,f**).

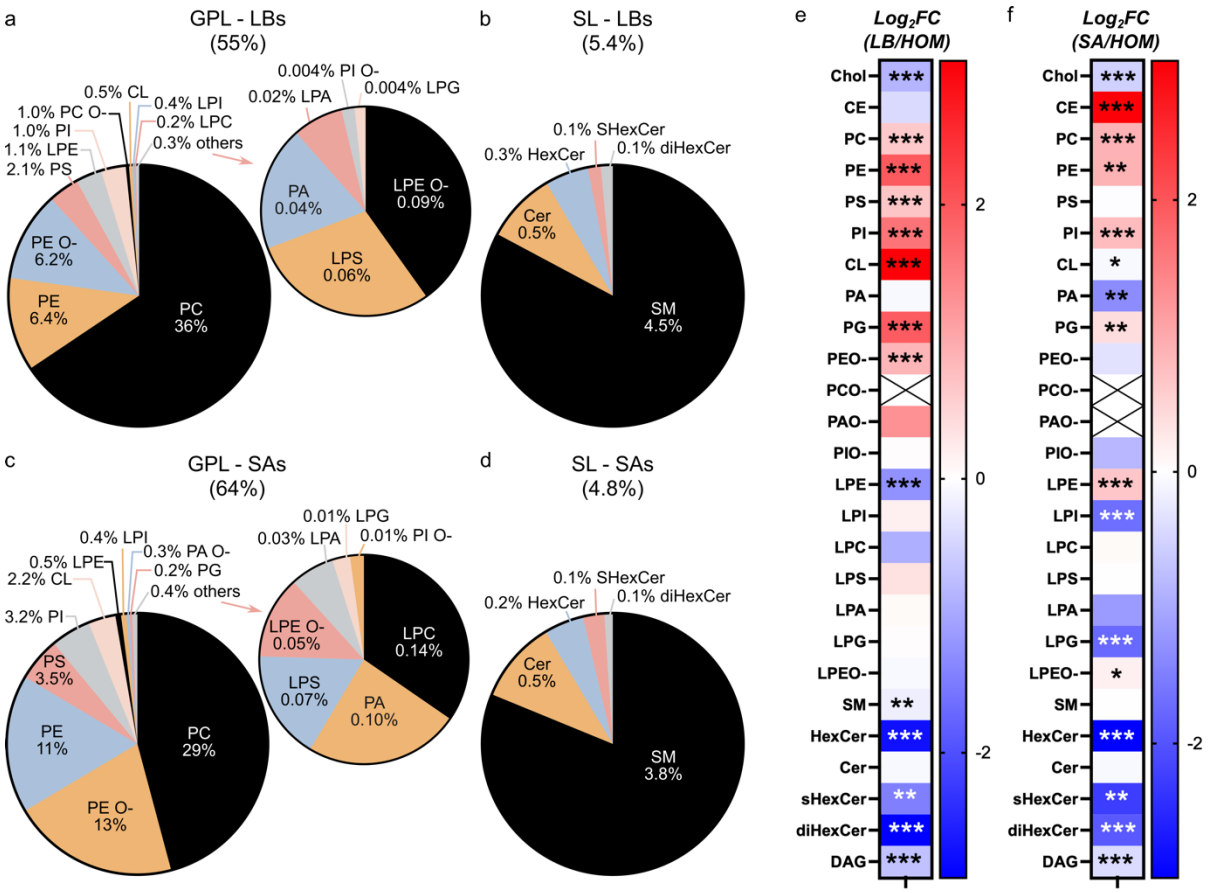

Figure 4: The lipid composition of LB- and SA-enriched fraction differs from that of amygdala homogenates. a-d. Species distribution of GPL (a,c) and SL (b,d) in amygdala LB- (a,b) and SA- (c,d) enriched fractions. e,f. Heat maps showing log_2FC in the levels of lipid classes in LB- (e) and SA- (f) enriched fractions. The asterisks indicate the p-value for the t-test comparison LB vs homogenates (e) or SA vs homogenates (f). *p<0.033, **p<0.002, ***p<0.001

The analyses of the lipid classes using the same approach as that described above for the homogenates showed that both long sPD and risk *GBA* mutations mainly led to the systematic increase in the levels of HexCer, Cer, SHexCer, diHexCer and/or GalCer in both LB- and SA-enriched fractions relative to their levels in $sPD_{<30y}$ and sPD_{ddm}, respectively (**Fig. 5a,b and 6a,b,** respectively). We note that long sPD and risk *GBA* mutations are associated with the same lipid changes in homogenates, LBs, and SAs (Fig. 1k). Still, the number of lipid classes with significantly affected levels is much lower and limited to SL for LBs and SAs compared to homogenates. Long sPD and *GBA* risk mutations led to the same changes in the species distribution of GPL and SL in LBs and SAs as observed in homogenates (**Fig. 5c-q and 6c-q**, respectively). Again, less species were affected in LB- and SA-

enriched fraction than in homogenates. In both fractions, long sPD and *GBA* risk mutations led to the decrease in the levels of SM/Cer 36:1, HexCer 42:2, PA/PE/PS 40:6, PE O- 40:7 and an increase in the levels of HexCer 36:1, GalCer 42:2, SM/Cer 42:2, PS 36:1, PE O- 36:3 relative to their levels in $sPD_{<30y}$ and sPD_{ddm}, respectively (**Fig. 5c-q and 6c-q**, respectively).

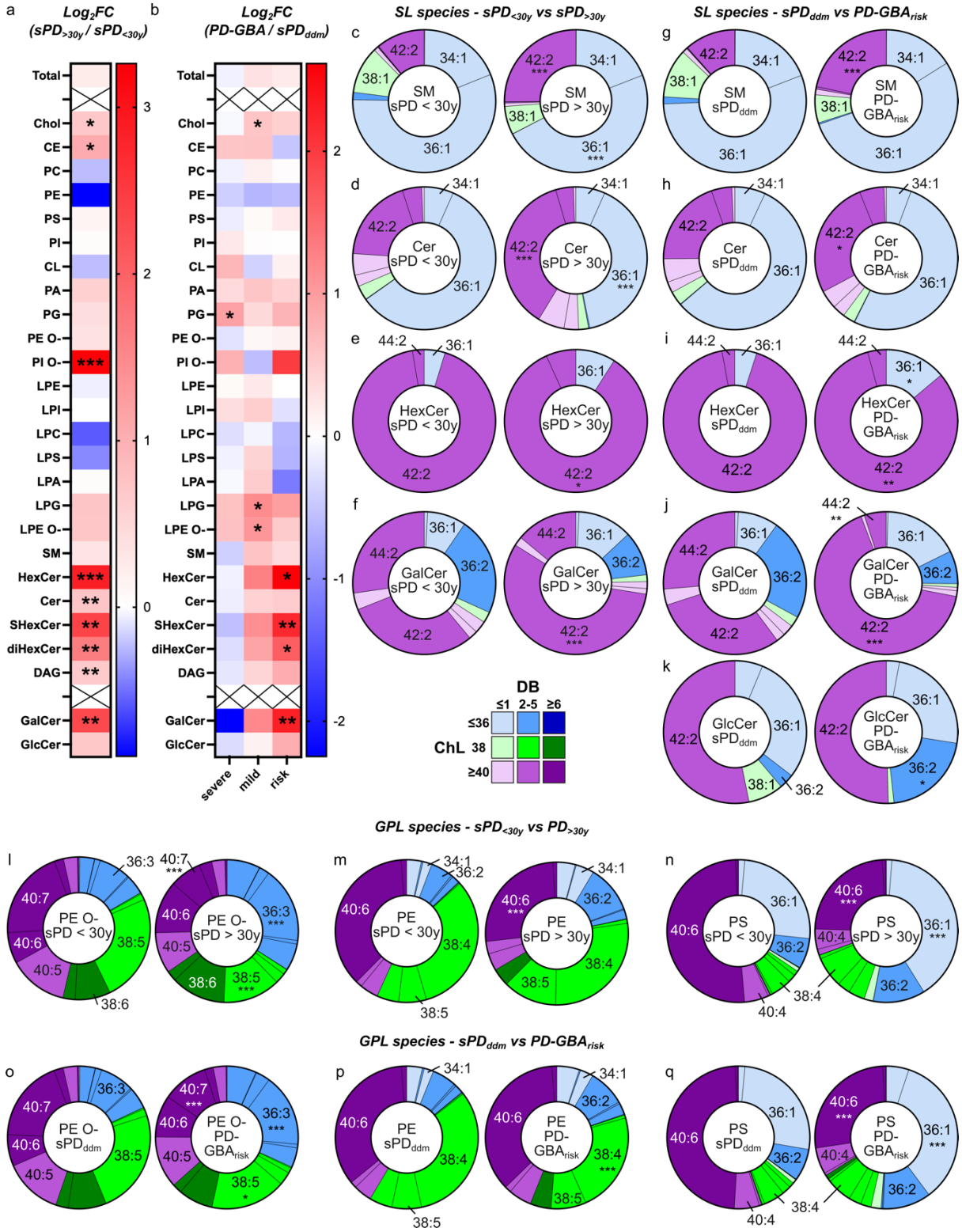

Figure 5: Long sPD and *GBA* risk mutations lead to changes in the levels of lipid classes and species in LB-enriched fractions that are similar to those observed in homogenates. a,b. Heat map showing log_2FC in the levels of lipid classes associated with long sPD (a) or *GBA* severe, mild or risk mutations (b). The asterisks indicate the p-value for the t-test comparisons $sPD_{<30y}$ (n = 15) vs $sPD_{>30y}$ (n = 5) (a) or *GBA* (severe (n = 4), or mild (n = 5) or risk (n = 6)) vs sPD_{ddm} cases (n = 13) (b). c-q. Pie charts showing the species distribution for SM (c,g), Cer (d,h), HexCer (e,i), GalCer (f,j), GlcCer (k), PE O- (l,o), PE (m,p) and PS (n,q) in $sPD_{<30y}$ (left, c-f, l-n), $sPD_{>30y}$ (right, c-f, l-n), sPD_{ddm} (left, g-k, o-q) and PD-GBA_{risk} (right, g-k, o-q) cases. The asterisks indicate the p-value for two-way ANOVA with Šidák multiple comparison test between the mean in PD-GBA_{risk} and that for PD_{ddm} or the mean in $sPD_{<30y}$ and that for $sPD_{>30y}$ for each lipid specie (% of total class). Only lipid classes for which significant changes in their species distribution were observed in association with long sPD or PD-GBA_{risk} are shown. *p<0.0332, **p<0.0021, ***p<0.0002.

Such changes in the lipid distribution led to the same changes in average ChL and DB due to long sPD and *GBA* risk mutation in LB- and SA-enriched fractions as those observed in homogenates (**Fig. S13**). We found that the average ChL and DB of PS, PE O- were both decreased and the average ChL and DB of SM and Cer were both increased in both LB and SA in association with long sPD whereas either one or the other was observed in PD-GBA_{risk} cases (**Fig. S13**).

Altogether, we found that long sPD and *GBA* risk mutation led to the same changes in the levels and species distribution of GPL and SL in SA- and LB-enriched fractions as those observed in homogenates, but the number of lipids affected is smaller in SA- and LB-enriched fractions than in homogenates. These results suggest that the SAs and LBs differ less from one group to another (sPD with different disease duration, PD-GBA_{severe}, PD-GBA_{mild}, and PD-GBA_{risk}) and are more homogeneous in terms of their lipid composition, GCase activity, and protein levels as well as pSer-αS levels, than homogenates.

Discussion

Increasing evidence points towards a role of disruptions in lipid metabolism in the emergence and spreading of αS pathology in PD[17,18]. Changes in the levels of specific lipids such as Chol, fatty acids and SL have been observed in association with changes in the levels of total, oligomeric and/or pathological αS in cellular and animal models of PD as well as in patient-derived samples from PD patients[17,18]. Mutations in the *GBA* gene, encoding GCase, are, altogether, the most important genetic risk factor for PD and are associated with a decrease in the protein and/or activity levels of GCase, lysosomal dysfunction and/or accumulation of pathological αS and/or the GCase substrate, GlcCer and GlcSph in fibroblasts, CSF and post-mortem brain samples[18–20]. A decrease in GCase activity has been reported not only in samples from PD-GBA patients but also in samples from patients with sPD[18]. Different brain areas are affected to different extents by such a decrease GCase activity and/or protein levels and associated increases in pathological αS and specific lipids[18]. In this study, we investigated the interplay between GCase, αS, and lipids in amygdala homogenates from sPD patients with different disease duration and PD-GBA patients with different *GBA* mutations. We chose to work with amygdala

samples as this brain area is affected by high αS pathology with limited neuronal loss[50]. Moreover, amygdala is affected at different stages in the body-first vs brain-first model making this brain area central to the understanding of these two types of PD[51,52].

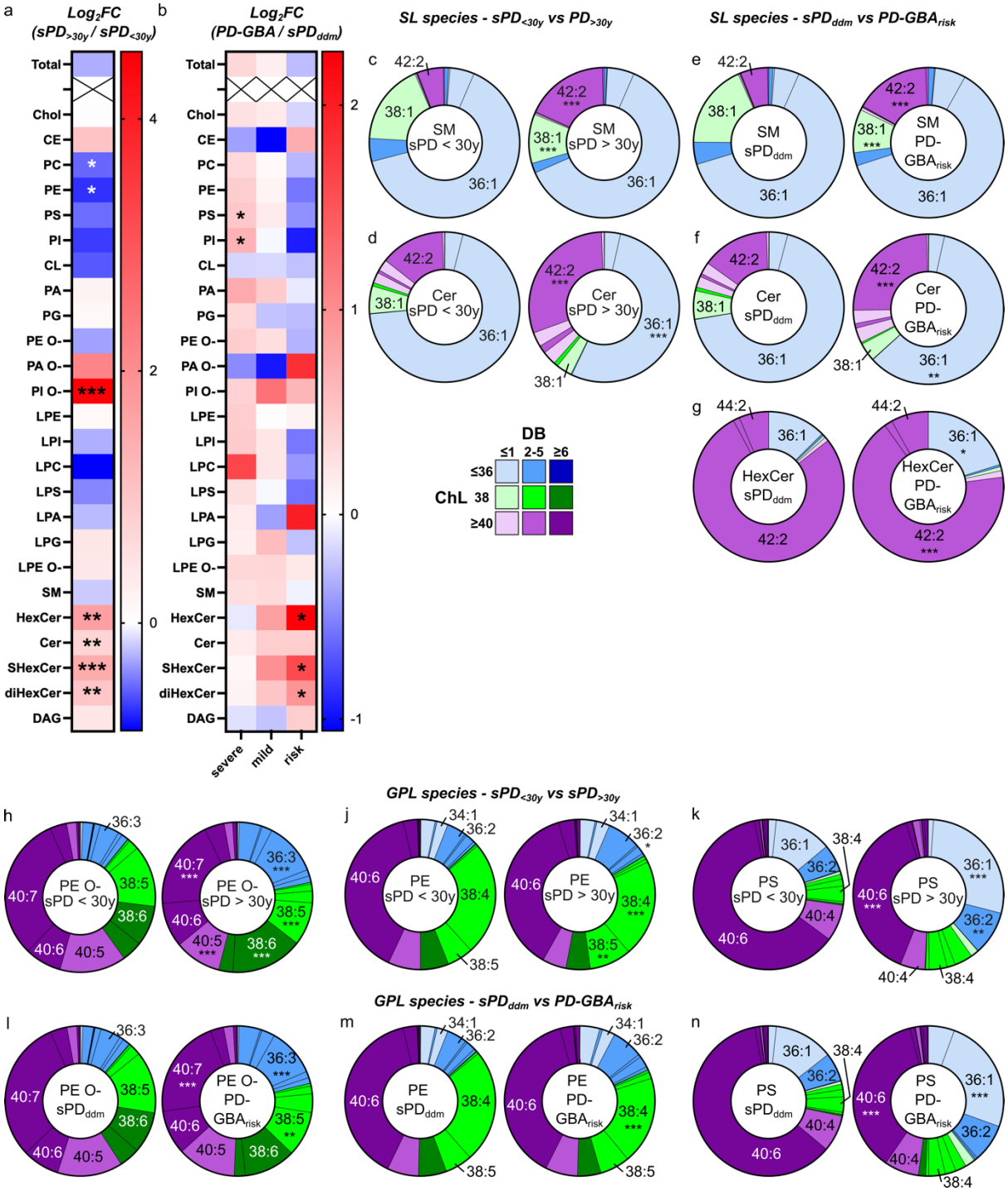

Figure 6: Long sPD and *GBA* risk mutations lead to changes in the levels of lipid classes and species in SA-enriched fractions that are similar to those observed in homogenates. a,b. Heat map showing log_2FC in the levels of lipid classes associated with long sPD (a) or *GBA* severe, mild or risk mutations (b). The asterisks indicate the p-value for the t-test comparisons $sPD_{>30y}$ (n = 5) vs $sPD_{<30y}$ (n = 15) (a) or PD-GBA (severe (n = 4), or mild (n = 5) or risk (n = 6)) vs sPD_{ddm} cases (n = 13) (b). c-g. Pie charts showing the species distribution for SM (c,e), Cer (d,f), HexCer (g), PE O- (h,j), PE (j,m)

and PS (k,n) in $sPD_{<30y}$ (left, c,d, h-k), $sPD_{>30y}$ (right, c,d, h-k), sPD_{ddm} (left, e-g, l-n) and PD-GBA_{risk} (right, e-g, l-n) cases. The asterisks indicate the p-value for two-way ANOVA with Šidák multiple comparison test between the mean in PD-GBA_{risk} and that for sPD_{ddm} or the mean in $sPD_{<30y}$ and that for $sPD_{>30y}$ for each lipid specie (% of total class). Only lipid classes for which significant changes in their species distribution were observed in association with long sPD or PD-GBA_{risk} are shown. *p<0.0332, **p<0.0021, ***p<0.0002.

Finally, we analysed homogenates and αS aggregates (LB- and SA-enriched fractions) to investigate potential changes in the composition of these protein-lipid co-assemblies with disease duration or with *GBA* mutations.

Our combined lipidomic and biochemical analyses of amygdala homogenates from sPD and PD-GBA patients show that sPD disease duration above 30 y (long sPD) and *GBA* risk mutations (i.e. p.E365K and p.T408M) lead to a decrease in the levels of GCase activity and protein and CL as well as an increase in the levels of pathological αS, total lipid, most GPL, Chol and SL relative to those in $sPD_{<30y}$ and sPD_{ddm} cases, respectively. Long sPD and *GBA* risk mutations also disrupt the distribution of GPL and SL species and led to a shift from long more unsaturated to short more saturated GPL and to longer SM/Cer. Interestingly, our results show that *GBA* mild mutation (i.e. p.N409S) affects the levels of the same lipids and in the same direction as that observed for long sPD and *GBA* risk mutations but to a lesser extent whereas *GBA* severe mutation (i.e. p.L483P) affects the same lipids but in the opposite direction. For ex. the levels SM 36:1 and SM 42:2 were found to decrease and increase, respectively, in *GBA* risk and mild homogenates and the opposite was observed for *GBA* severe homogenates. Such an imbalance in the levels short and long SL were also observed in association with PD-GBA severe human fibroblasts[30,53]. In particular, we found that short chain SM and Cer (36:1 species) are increased in *GBA* severe amygdala homogenates as observed in the fibroblasts (SM and Cer 34:1)[30].

Long PD and *GBA* risk also led to the decrease of the levels and/or average ChL and DB of CL. CL is a major component of mitochondrial membranes[54] and is proposed to be involved in mitochondrial morphology, bioenergetics, dynamics, and signalling pathways[55]. Alterations in brain CL are associated with impaired neuronal function and neurodegeneration. Long PD and *GBA* risk mutations led to the increase in the levels of 72:5 CL and the decrease in those of 74:9 CL and as for the SL, the opposite was observed in *GBA* severe samples where the levels of 72:5 CL were decreased. Our results suggest that disruptions in the levels and properties of CL may be responsible for the reported mitochondrial dysfunction associated with *GBA* mutations in fibroblasts and induced pluripotent stem cell (iPSC)-derived neurons[56,57].

The levels of GCase activity, αS and lipids were found to correlate in sPD samples, reinforcing the hypothesis of an interplay between these three partners in PD[18]. Indeed, we have found such a

correlation when combining existing quantification of αS, GCase and lipid levels in iPSC-derived neurons and brain samples[18]. However, limited evidence is yet available to establish whether the relation among the levels of GCase, αS and lipids are the cause or consequence of PD.

LBs are complex structures made of organelles such as mitochondria and lysosomes, lipid and protein molecules, whose formation have been linked to PD and αS pathology[58]. We found that both αS and GCase were present in both LB- and SA-enriched fractions and that their activity and/or protein levels did not change among the different investigated groups, i.e. $sPD_{>30y}$ vs $sPD_{<30y}$; sPD_{ddm} vs $PD\text{-}GBA_{severe}$, $PD\text{-}GBA_{mild}$ and $PD\text{-}GBA_{risk}$. Our lipid analysis shows the presence of CL, a lipid exclusively found in mitochondria, in both of these fractions, suggesting the presence of mitochondria in these protein-lipid inclusions, as previously shown for LBs[2]. The other lipid detected in these preparations (**Fig. S15 and S16**) include previously reported lipids found in micro dissected LBs such as PC 32:0 and PC 34:1, SM 36:1 (SM 18:1/18:0), SM 38:1 (SM18:1/20:0) and SM 42:2 (SM 28:1/24:1)[2]. Moreover, LB- and SA-enriched fractions had higher percentages in specific lipids including relative long chain phospholipids (PE 40:6, PS 40:6, PE O- 40:7) and HexCer (42:2) and relative short chain PC (32:0) and SM (36:1) than homogenates (**Fig S14-S16**), suggesting that these lipids either preferentially co-assemble with αS into SAs and LBs or that they are main components of membranes or organelles that are involved in the formation of SAs and LBs. As observed for αS and GCase, LB- and SA- enriched fractions varied less in term of their lipid composition among the different investigated groups ($sPD_{<30y}$ vs $sPD_{>30y}$, sPD_{ddm} vs PD-GBA) than homogenates. Mainly the levels of specific SL (36:1, 38:5 and 42:2 SM, Cer and/or HexCer) and GPL (36:1, 36:2, 36:3, 38:4 and/or 42:2 PE O-, PS and/or PE) were changed in long sPD and PD-GBA cases, relative to those in $sPD_{<30y}$ and sPD_{ddm} cases, respectively. These results suggest that LB- and SA-enriched fractions are more homogeneous in their protein and lipid composition than homogenates. This finding suggests that the formation of LBs or SAs is likely to occur via the same reaction in the brain of different individuals, i.e. via co-assembly of a given number of molecules of proteins with a given number of lipid molecules, and that increases in the levels of αS and lipid substrates are likely to increase the rate at which the reaction occurs rather than affecting the composition of the end product of the reaction, i.e. LBs or SAs.

Finally, our results show that each *GBA* mutation led to specific changes in the lipidome of PD amygdala homogenates that vary in their magnitude and direction from one *GBA* mutation category to another, i.e. severe, mild, risk. This observation suggests that substrate alternating approach aiming at reverting

lipid changes associated with a given *GBA* mutation might benefit a group of *GBA* mutations like *GBA* mild and risk, but would result in worst outcome for another *GBA* group, like *GBA* severe. These results reinforce the need for patients stratification that may explain previous failure in clinical trials (e.g. Venglusat[59]).

Materials and methods

Purification of Lewy bodies from human PD brains

The brain samples were obtained from Queen Square Brain Bank for Neurological Disorders (London, UK) following local research approval. All cases met the UK Brain Bank clinical and pathological criteria for PD and have informed consent for material usage for medical research. Amygdala tissue were dissected from fresh frozen post-mortem brains from a total of 35 patients (20 x sPD and 15 x PD-GBA (5x p.N409S, 4x p.E365K, 4x p.L483P and 2x p.T408M). The two groups were matched for age as shown in Table 1.

Table 1. Demographic details of the patients included in the study

		N	Sex	Age of death (years)	Age of onset (years)	Disease duration (years)
sPD	**Total**	**20**	**10F:10M**	**76.5 ± 8.6**	**56.6 ± 14.4**	**19.9 ± 10.6**
	<10	4	2F:2M	80.0 ± 10.7	74.5 ± 11.7	5.5 ± 1.3
	11-20	6	3F:3M	74.7 ± 9.4	60.7 ± 11.3	14.0 ± 3.3
	21-30	5	3F:2M	74.6 ± 9.3	49.6 ± 7.9	25.0 ± 2.4
	>30	5	2F:3M	77.6 ± 7.0	45.3 ± 8.4	33.2 ± 1.8
PD-GBA	**Total**	**15**	**4F:11M**	**76.4 ± 11.2**	**61.7 ± 12.1**	**14.7 ± 5.3**
	p.N409S	5	5M	83.8 ± 4.4	68.2 ± 8.3	15.6 ± 6.5
	p.L483P	4	2F:2M	59.5 ± 5.2	45.3 ± 8.7	14.3 ± 6.9
	p.E365K	4	1F:3M	81.5 ± 3.0	68.5 ± 3.5	13.0 ± 3.7
	p.T408M	2	1F:1M	81.5 ± 2.1	65.0 ± 1.4	16.5 ± 3.5

Purification of LBs and SAs was performed as in Cavaliere et al, 2017[60] with minor differences. In summary, tissue was homogenized in 15 µl/mg ice-cold MSE buffer (10 mM MOPS/KOH, pH 7.4, 1 M sucrose, 1 mM EGTA and 1 mM EDTA) with protease inhibitor cocktail (Complete Mini; Boehringer Mannheim) with a manual Glass Pestle Tissue Grinder. Before purification, a small fraction of homogenate was collected to use as whole amygdala homogenate. For LB and SA purification, a sucrose gradient was prepared by overlaying 2.2 M with 1.4 M and finally with 1.2 M sucrose in volume rations of 3.5:8:8 (v/v). The homogenate was layered on the gradient and centrifuged (3h, 4°C, 160,000

xg) using a SW40 rotor (Beckman). Top layer of debris was removed and ~18 fractions of 500 µl were collected from each gradient from top (fraction 1) to bottom (fraction 18). Detection for the presence of αS aggregated in each fraction was performed using filter retardation assay, as previously described[48]. The selected fractions were also visualized under the microscope to confirm the presence of LB and the purity of the samples.

BCA Assay

Total protein content was measured in homogenate, LB- and SA-enriched samples using the Pierce BCA Protein Assay Kit (Thermo Fisher Scientific, 23225) following the manufacturer's protocol.

Lipidomics

25 µg of each homogenate and LB-enriched sample was mixed with 155 mM Ammonium Bicarbonate (AB, Sigma-Aldrich, FL40867) to 200 µl and sonicated for 30 min in a water-bath sonicator. For SA-enriched samples 20 µg was diluted in 220 µl with AB buffer and mixed and used for lipid extraction directly. Lipid extraction and shotgun lipidomics was done using quantitative MS-based shotgun lipidomics. Each sample was spiked with a 10x Internal Standard Mix with a known content of a variety of different lipids[61] and a GalCer Standard Mix. Organic solvents containing mixture of chloroform and methanol (C/M 2:1, 1 ml) was added to the sample which was then mixed (15 min, 4°C, 2000 rpm) and centrifuged (2 min, 4°C, 2000 xg). The organic phase was isolated and for homogenate and LB-enriched samples two rounds of cleaning were performed by adding methanol (100 µl) and AB (50 µl), mixed (5 min, 4°C, 2000 rpm) and centrifuged (2 min, 4°C, 2000 xg). The organic phase was transferred to a new tube and evaporated for 1 h. The lipid film was dissolved in C/M (1:2 v/v, 100 µl) by mixing (5 min, 4°C, 2000 rpm) and then centrifuged (15 min, 4°C, 15000 xg). Each lipid extract was mixed with positive and negative solvents (13.3 mM AB in 2-propanol or 0.2% (v/v) tri-ethyl-amine in chloroform/methanol 1:5 (v/v), respectively) and analyzed in the positive and negative ion modes on quadrupole-Orbitrap mass spectrometer Q Exactive (Thermo Fisher Scientific) equipped with TriVersa NanoMate (Advion Biosciences) for automated and direct nanoelectrospray infusion, as described previously[61]. In addition 50 µl of each sample was transferred into a new tube, evaporated for 30 min and dissolved in 50 µl of CAN to further quantify GlcCer.

We considered a lipid specie to be detected, and thereby to be included in the processing of the full dataset, if its level was a nonzero value in more than half of the total number of samples per group.

Western blot

Protein content of homogenate, LB- and SA-enriched samples were measured using the Pierce TM BCA Protein Assay Kit (Thermo Fisher Scientific, 23225). Samples of 20 µg (homogenates), 5 µg (LB) or 10 µg (SA) total protein were electrophoresed on a NuPage 4%-12% Bis-Tris Protein gel (Thermo Fisher Scientific) in a randomised order. Due to shortage in material, only 31 out of the total of 35 LB-enriched samples were included (**Fig. S7**). Also, for three SA enriched samples, due to low protein concentration, lower protein amounts were loaded: $PD_{GBA\ severe1}$ 4.5 µg, $sPD_{20\text{-}30.3}$ 4.4 µg and $sPD_{20\text{-}30.2}$ 6.5 µg. Proteins were transferred to a PVDF membrane (0.2 µm, Thermo Fisher Scientific, 88520), blocked in 5% w/v milk (2 h) and treated with primary and secondary antibodies. Antibody binding was detected using an ECL chemiluminescence kit (Bio-Rad, 1705061). In order to detect multiple proteins for the same set of samples, the membrane was stained multiple times. Firstly, the full membrane was stained for pSer-αS and imaged, then the membrane was reactivated in methanol, stripped with acetic buffer (0.015 % w/v glycine, 0.001 % w/v SDS and 1% v/v Tween-20, pH 2.2), blocked in 5% w/v milk (2 h), reprobed with next antibody and imaged. Second reprobe was for total αS and third for GCase (only top part of membrane stained, >50 kDa) and β-act (only bottom part of membrane stained, <50 kDa). The first membrane of the homogenates (#1) was cut so that parts of the β-actin bands were not shown for the bottom part of the membrane. Therefore, for this membrane only, another stripping and reprobing was performed after the staining for GCase on the top part of the membrane; the two membrane pieces were merged and stained for β-actin once more, in order to visualize the β-actin bands of the last 5 samples on the membrane.

The following antibodies were used: pSer129-αS (CST, 23706, 1:1000), α-synuclein (BD Biosciences, 610787, 1:500), β-actin (ABclonal, AC026, 1:100.000), GBA (Abcam, ab55080, 1:1000), anti-mouse (Abcam, ab205719, 1:5000) and anti-rabbit (Abcam, ab6721, 1:5000).

GCase activity assay

Samples of brain homogenates were diluted to a concentration of 0.1 mg/ml, LB-enriched samples to 0.02 mg/ml and SA-enriched samples to 0.0925 mg/ml in reaction buffer (0.1 M sodium citrate, 0.1% Triton X-100, 6.5 M sodium taurocholate, 2.5 mM 4-methylumbelliferyl β-D-glucopyranoside) and incubated in non-binding plates (Corning 3881) while shaking (37°C).

Solutions with varying concentrations of 4-methylumbelliferone, from 0 to 50 µM for homogenate samples from 0 to 25 µM for LB-enriched samples and from 0 to 12.5 µM for SA-enriched samples, also diluted in reaction buffer, were analysed under same conditions to convert fluorescence units into µM

of 4-methylumbelliferone. Fluorescence was measured using CLARIOstar plate reader (BMG Labtech, Aylesbury, UK) with excitation/emission filters of 360-20/450-10 nm. The GCase activity was calculated using following equation:

$$Activity\left(\frac{\frac{nmol}{h}}{mg}\right)=\frac{\frac{\Delta fl}{\Delta t}}{\Delta std * C_{prot}}$$

Where $\Delta fl/\Delta t$ is the change in fluorescence per hour, Δstd is the change in fluorescence (fluorescence unit) per concentration 4-methylumbelliferone (μM) and C_{prot} is the total protein concentration of the solution, 0.05 mg/ml.

Statistics

Statistical analysis and graph visualisation were performed using Prism 9 software (GraphPad). Statistical significance, when comparing the mean of two groups, was determined using unpaired t-test. Comparisons among three groups or more was performed using One-way ANOVA and multiple *t*-test comparisons (Šídák's multiple comparisons test). Comparisons with a p-value below 0.05 were considered statistically significant. Data were shown as mean ± SEM for all results. Abundance of lipid classes and species were illustrated as Pearson r coefficients in heat maps and effects achieving $p < 0.033$ were interpreted as statistically significant. Correlation graphs were analysed using simple linear regression, with $p < 0.05$ interpreted as a significant correlation between the two tested variables.

References:

1. Damier, P., Hirsch, E. C., Agid, Y. & Graybiel, A. M. The substantia nigra of the human brain: II. Patterns of loss of dopamine-containing neurons in Parkinson's disease. *Brain* **122**, 1437–1448 (1999).
2. Shahmoradian, S. H. *et al.* Lewy pathology in Parkinson's disease consists of crowded organelles and lipid membranes. *Nat. Neurosci.* **22**, 1099–1109 (2019).
3. Spillantini, M. G. *et al.* α-Synuclein in Lewy bodies. *Nature* **388**, 839–840 (1997).
4. Theillet, F.-X. *et al.* Structural disorder of monomeric α-synuclein persists in mammalian cells. *Nature* **530**, 45–50 (2016).
5. Burré, J. *et al.* Properties of native brain α-synuclein. *Nature* **498**, E4–E6 (2013).
6. Fusco, G. *et al.* Direct observation of the three regions in α-synuclein that determine its membrane-bound behaviour. *Nat. Commun.* **5**, 3827 (2014).
7. Bendor, J. T., Logan, T. P. & Edwards, R. H. The Function of α-Synuclein. *Neuron* **79**, 1044–1066 (2013).
8. Fink, A. L. The Aggregation and Fibrillation of α-Synuclein. *Acc. Chem. Res.* **39**, 628–634 (2006).
9. Galvagnion, C. *et al.* Lipid vesicles trigger α-synuclein aggregation by stimulating primary nucleation. *Nat. Chem. Biol.* **11**, 229–234 (2015).
10. Grey, M. *et al.* Acceleration of α-Synuclein Aggregation by Exosomes*. *J. Biol. Chem.* **290**, 2969–2982 (2015).
11. Martinez, Z., Zhu, M., Han, S. & Fink, A. L. GM1 Specifically Interacts with α-Synuclein and Inhibits Fibrillation. *Biochemistry* **46**, 1868–1877 (2007).
12. Zhu, M. & Fink, A. L. Lipid Binding Inhibits α-Synuclein Fibril Formation*. *J. Biol. Chem.* **278**, 16873–16877 (2003).

13. Galvagnion, C. *et al.* Chemical properties of lipids strongly affect the kinetics of the membrane-induced aggregation of α-synuclein. *Proc. Natl. Acad. Sci.* **113**, 7065–7070 (2016).

14. Galvagnion, C. *et al.* Lipid Dynamics and Phase Transition within α-Synuclein Amyloid Fibrils. *J. Phys. Chem. Lett.* **10**, 7872–7877 (2019).

15. Hellstrand, E., Nowacka, A., Topgaard, D., Linse, S. & Sparr, E. Membrane Lipid Co-Aggregation with α-Synuclein Fibrils. *PLOS ONE* **8**, e77235 (2013).

16. Galvagnion, C. *et al.* Structural characterisation of α-synuclein–membrane interactions and the resulting aggregation using small angle scattering. *Phys. Chem. Chem. Phys.* **26**, 10998–11013 (2024).

17. Galvagnion, C. The Role of Lipids Interacting with α-Synuclein in the Pathogenesis of Parkinson's Disease. *J. Park. Dis.* **7**, 433–450 (2017).

18. Muñoz, S. S., Petersen, D., Marlet, F. R., Kücükköse, E. & Galvagnion, C. The interplay between Glucocerebrosidase, α-synuclein and lipids in human models of Parkinson's disease. *Biophys. Chem.* **273**, 106534 (2021).

19. Gegg, M. E. & Schapira, A. H. V. The role of glucocerebrosidase in Parkinson disease pathogenesis. *FEBS J.* **285**, 3591–3603 (2018).

20. Schapira, A. H. V., Chiasserini, D., Beccari, T. & Parnetti, L. Glucocerebrosidase in Parkinson's disease: Insights into pathogenesis and prospects for treatment. *Mov. Disord.* **31**, 830–835 (2016).

21. Sidransky, E. *et al.* Multi-center analysis of glucocerebrosidase mutations in Parkinson disease. *N. Engl. J. Med.* **361**, 1651–1661 (2009).

22. Gan-Or, Z. *et al.* Differential effects of severe vs mild GBA mutations on Parkinson disease. *Neurology* **84**, 880–887 (2015).

23. Parlar, S. C., Grenn, F. P., Kim, J. J., Baluwendraat, C. & Gan-Or, Z. Classification of GBA1 variants in Parkinson's disease; the GBA1-PD browser. *Mov. Disord. Off. J. Mov. Disord. Soc.* **38**, 489–495 (2023).

24. Mallett, V. *et al.* GBA p.T369M substitution in Parkinson disease: Polymorphism or association? A meta-analysis. *Neurol. Genet.* **2**, e104 (2016).

25. Duran, R. *et al.* The Glucocerobrosidase E326K Variant Predisposes to Parkinson's Disease, But Does Not Cause Gaucher's Disease. *Mov. Disord. Off. J. Mov. Disord. Soc.* **28**, 232–236 (2013).

26. Schöndorf, D. C. *et al.* iPSC-derived neurons from GBA1-associated Parkinson's disease patients show autophagic defects and impaired calcium homeostasis. *Nat. Commun.* **5**, 4028 (2014).

27. Ambrosi, G. *et al.* Ambroxol-induced rescue of defective glucocerebrosidase is associated with increased LIMP-2 and saposin C levels in *GBA1* mutant Parkinson's disease cells. *Neurobiol. Dis.* **82**, 235–242 (2015).

28. Sanchez-Martinez, A. *et al.* Parkinson disease-linked GBA mutation effects reversed by molecular chaperones in human cell and fly models. *Sci. Rep.* **6**, 31380 (2016).

29. Collins, L. M., Drouin-Ouellet, J., Kuan, W.-L., Cox, T. & Barker, R. A. Dermal fibroblasts from patients with Parkinson's disease have normal GCase activity and autophagy compared to patients with PD and GBA mutations. Preprint at https://doi.org/10.12688/f1000research.12090.2 (2018).

30. Galvagnion, C. *et al.* Sphingolipid changes in Parkinson L444P GBA mutation fibroblasts promote α-synuclein aggregation. *Brain* **145**, 1038–1051 (2022).

31. Sun, Y. *et al.* Properties of Neurons Derived from Induced Pluripotent Stem Cells of Gaucher Disease Type 2 Patient Fibroblasts: Potential Role in Neuropathology. *PLOS ONE* **10**, e0118771 (2015).

32. Yang, S., Gegg, M., Chau, D. & Schapira, A. Glucocerebrosidase activity, cathepsin D and monomeric α-synuclein interactions in a stem cell derived neuronal model of a PD associated *GBA1* mutation. *Neurobiol. Dis.* **134**, 104620 (2020).

33. Yang, S.-Y., Beavan, M., Chau, K.-Y., Taanman, J.-W. & Schapira, A. H. V. A Human Neural Crest Stem Cell-Derived Dopaminergic Neuronal Model Recapitulates Biochemical Abnormalities in *GBA1* Mutation Carriers. *Stem Cell Rep.* **8**, 728–742 (2017).

34. Fernandes, H. J. R. *et al.* ER Stress and Autophagic Perturbations Lead to Elevated Extracellular α-Synuclein in *GBA-N370S* Parkinson's iPSC-Derived Dopamine Neurons. *Stem Cell Rep.* **6**, 342–356 (2016).

35. Woodard, C. M. *et al.* iPSC-Derived Dopamine Neurons Reveal Differences between Monozygotic Twins Discordant for Parkinson's Disease. *Cell Rep.* **9**, 1173–1182 (2014).

36. Burbulla, L. F. *et al.* A modulator of wild-type glucocerebrosidase improves pathogenic phenotypes in dopaminergic neuronal models of Parkinson's disease. *Sci. Transl. Med.* **11**, eaau6870 (2019).

37. Rocha, E. M. *et al.* Progressive decline of glucocerebrosidase in aging and Parkinson's disease. *Ann. Clin. Transl. Neurol.* **2**, 433–438 (2015).

38. Huebecker, M. *et al.* Reduced sphingolipid hydrolase activities, substrate accumulation and ganglioside decline in Parkinson's disease. *Mol. Neurodegener.* **14**, 40 (2019).

39. Gegg, M. E. *et al.* Glucocerebrosidase deficiency in substantia nigra of parkinson disease brains. *Ann. Neurol.* **72**, 455–463 (2012).

40. Gegg, M. E. *et al.* No evidence for substrate accumulation in Parkinson brains with GBA mutations. *Mov. Disord.* **30**, 1085–1089 (2015).

41. Boutin, M., Sun, Y., Shacka, J. J. & Auray-Blais, C. Tandem Mass Spectrometry Multiplex Analysis of Glucosylceramide and Galactosylceramide Isoforms in Brain Tissues at Different Stages of Parkinson Disease. *Anal. Chem.* **88**, 1856–1863 (2016).

42. Braak, H. *et al.* Amygdala pathology in Parkinson's disease. *Acta Neuropathol. (Berl.)* **88**, 493–500 (1994).

43. Harding, A. J., Stimson, E., Henderson, J. M. & Halliday, G. M. Clinical correlates of selective pathology in the amygdala of patients with Parkinson's disease. *Brain* **125**, 2431–2445 (2002).

44. Sorrentino, Z. A. *et al.* Unique α-synuclein pathology within the amygdala in Lewy body dementia: implications for disease initiation and progression. *Acta Neuropathol. Commun.* **7**, 142 (2019).

45. Dasgupta, S. & Ray, S. K. Diverse Biological Functions of Sphingolipids in the CNS: Ceramide and Sphingosine Regulate Myelination in Developing Brain but Stimulate Demyelination during Pathogenesis of Multiple Sclerosis. *J. Neurol. Psychol.* **5**, 10.13188/2332-3469.1000035 (2017).

46. Iwatsubo, T. *et al.* Purification and characterization of Lewy bodies from the brains of patients with diffuse Lewy body disease. *Am. J. Pathol.* **148**, 1517–1529 (1996).

47. Kramer, M. L. & Schulz-Schaeffer, W. J. Presynaptic α-Synuclein Aggregates, Not Lewy Bodies, Cause Neurodegeneration in Dementia with Lewy Bodies. *J. Neurosci.* **27**, 1405–1410 (2007).

48. Recasens, A. *et al.* Lewy body extracts from Parkinson disease brains trigger α-synuclein pathology and neurodegeneration in mice and monkeys. *Ann. Neurol.* **75**, 351–362 (2014).

49. Bourdenx, M. *et al.* Identification of distinct pathological signatures induced by patient-derived α-synuclein structures in nonhuman primates. *Sci. Adv.* **6**, eaaz9165 (2020).

50. Fu, Y. *et al.* Increased unsaturated lipids underlie lipid peroxidation in synucleinopathy brain. *Acta Neuropathol. Commun.* **10**, 165 (2022).

51. Borghammer, P. The brain-first vs. body-first model of Parkinson's disease with comparison to alternative models. *J. Neural Transm.* **130**, 737–753 (2023).

52. Horsager, J. & Borghammer, P. Brain-first vs. body-first Parkinson's disease: An update on recent evidence. *Parkinsonism Relat. Disord.* **122**, 106101 (2024).

53. Abbott, S. K. *et al.* Altered ceramide acyl chain length and ceramide synthase gene expression in Parkinson's disease. *Mov. Disord.* **29**, 518–526 (2014).

54. van Meer, G., Voelker, D. R. & Feigenson, G. W. Membrane lipids: where they are and how they behave. *Nat. Rev. Mol. Cell Biol.* **9**, 112–124 (2008).

55. Falabella, M., Vernon, H. J., Hanna, M. G., Claypool, S. M. & Pitceathly, R. D. S. Cardiolipin, Mitochondria, and Neurological Disease. *Trends Endocrinol. Metab.* **32**, 224–237 (2021).

56. Schöndorf, D. C. *et al.* The NAD+ Precursor Nicotinamide Riboside Rescues Mitochondrial Defects and Neuronal Loss in iPSC and Fly Models of Parkinson's Disease. *Cell Rep.* **23**, 2976–2988 (2018).

57. García-Sanz, P. *et al.* N370S-GBA1 mutation causes lysosomal cholesterol accumulation in Parkinson's disease. *Mov. Disord.* **32**, 1409–1422 (2017).

58. Fares, M. B., Jagannath, S. & Lashuel, H. A. Reverse engineering Lewy bodies: how far have we come and how far can we go? *Nat. Rev. Neurosci.* **22**, 111–131 (2021).

59. Giladi, N. *et al.* Safety and efficacy of venglustat in *GBA1*-associated Parkinson's disease: an international, multicentre, double-blind, randomised, placebo-controlled, phase 2 trial. *Lancet Neurol.* **22**, 661–671 (2023).

60. Cavaliere, F. *et al.* In vitro α-synuclein neurotoxicity and spreading among neurons and astrocytes using Lewy body extracts from Parkinson disease brains. *Neurobiol. Dis.* **103**, 101–112 (2017).

61. Nielsen, I. Ø. *et al.* Comprehensive Evaluation of a Quantitative Shotgun Lipidomics Platform for Mammalian Sample Analysis on a High-Resolution Mass Spectrometer. *J. Am. Soc. Mass Spectrom.* **31**, 894–907 (2020).